Journal of Harbin Engineering University
ISSN: 1006-7043

Vol 45 No. 2
February 2024

Aerodynamics Analysis Comparison between NACA 4412 and Falco Air foils

Sayel M. Fayyad[1]*, Aiman Al Alawin[2],Omar A. Shabi[3], Zaid Abulghanam[4],Suleiman Abu-Ein[5], Abdel Salam Alsabagh[6], Taiseer Abu-Rahmeh[8], Mohannad O. Rawashdeh[7],Muntaser Momani[8], Waleed Momani[9], NaimRizq Alkawaldeh[10], and Omar Badran[11]

[1, 2,45,6,7,8,9,11]Department of Mechanical Engineering, Faculty of Engineering Technology, Al-Balqa Applied University, Amman, Jordan

[10]Mechanical Engineering Department, Zarqa University College, Al-Balqa Applied University

[3] Mechanical Engineering Department, Faculty of Engineering, King Abdualziz University

ABSTRACT

This article presents a comparison between the NACA 4412 airfoil and Falco airfoils. The focus is on conducting a comprehensive analysis of the geometries of the Falco UAV and NACA 4412 airfoil, as the shape of the airfoil plays a crucial role in determining lift and drag forces. A two-dimensional computational fluid dynamics (CFD) investigation was conducted utilizing the conventional k-epsilon model to assess the turbulence effects resulting from high airflow rates around the airfoil. The study examined the behavior of numerical streamlines around the two distinct geometries across a range of angles of attack from 0 to 120 degrees.To identify the optimal airfoil shape for unmanned aerial vehicles (UAVs), the stress distribution, velocity distribution, and coefficients of aerodynamic forces are computed at various angles of attack. This analysis aims to determine the airfoil shape that yields the most favorable results for UAV applications.

A comparative study of various airfoils was conducted to assess their suitability for engineering applications such as drones, and the Falco airfoil emerged as a promising candidate due to its superior lift-to-drag ratio. The study employed the computational simulation software ANSYS Fluent, which utilized Navier-Stokes and energy equations to predict the flow pattern around different airfoils. The Falco UAV airfoil demonstrated exceptional performance in terms of lift coefficient and lift-to-drag ratio, while maintaining an acceptable drag coefficient. In contrast to other airfoils with identical drag coefficients, the Falco UAV airfoil exhibited a significantly higher lift-to-drag ratio. The aerodynamic performance was greatly influenced by the angle of attack, with the most favorable outcomes observed at an angle of 12°. As the angle of attack increased, the areas of low pressure and weak flow progressively shifted from the lower surface to the upper surface, indicating a change in flow separation from the bottom to the top. It has been demonstrated that computational modeling using FLUENT yields results comparable to those obtained in a wind tunnel, providing both accuracy and cost savings by eliminating the need for extensive experimentation.

Keywords: Aerodynamics, Airfoils, NACA 4412 airfoil, ANSYS, simulation, Falco airfoil.

INTRODUCTION

The objective of this analysis is to numerically examine various types of airfoils, including wings and bluff bodies, using ANSYS software, and compare the results to determine the optimal design conditions for airfoils, particularly in terms of geometry. Two specific airfoils, namely NACA 4412 and the Falco airfoil, were selected for study. The primary focus of this paper is to conduct an ANSYS simulation to analyze the NACA 4412 and Falco airfoils, comparing their results under different aerodynamic conditions and airfoil geometries. An airfoil consists of both upper and lower surfaces, and it is interesting to note that despite the upper surface of a typical wing profile having more curvature than the lower surface, there is a higher density of streamlines above the wing. According to Bernoulli's principle, an increase in fluid speed corresponds to a decrease in pressure or potential energy. This principle aligns with the principle of energy conservation. Within a constant flow along a streamline, the sum of mechanical energy forms in a fluid remains constant at all points. It is important to differentiate between airfoil section properties and wing or aircraft properties due to the effect of the wing planform. Wing sections can vary from root to tip, incorporating taper, twist, and sweepback. The resulting aerodynamic characteristics of the wing are determined by the actions of each section along its span. The wing's efficiency is measured by the lift-to-drag (L/D) ratio, which varies with the angle of attack but reaches a maximum value at a specific angle. At this angle, the wing achieves its optimum efficiency. The airfoil shape plays a critical role in determining the wing's most efficient angle of attack and the level of efficiency achieved. Research indicates that for common usage, the maximum thickness of the most efficient airfoils is typically located approximately one-third of the way back from the leading edge of the wing. To achieve desired effects, high-lift wings and high-lift devices are designed by shaping the airfoils accordingly. Increasing wing chamber enhances the lift produced by an airfoil. The curvature above and below the chord line surface of an airfoil is referred to as camber. Positive camber occurs when the chord line departs inward, while negative camber occurs when it departs outward. Therefore, high-lift wings exhibit a significant positive camber on the upper surface and a slight negative camber on the lower surface. Wing flaps can approximate this configuration by enlarging the upper chamber and creating a negative lower chamber[1, 8-13].

-NACA 4412 and Falco airfoils

The NACA four-digit wing sections utilize a specific framework to define the profile, consisting of the following components:

1. One digit describing the maximum camber as a percentage of the chord
2. Another digit describing the distance of maximum camber from the airfoil leading edge in tens of percents of the chord
3. Two digits describing maximum thickness of the airfoil as percent of the chord [2].

-Falco –Italian airfoils

The FALCO UAV serves as the aerial component of a versatile surveillance system employed for diverse civil and military operations. When fully loaded, the UAV has a maximum take-off weight below 500 kilograms (1100 lbs). Key performance requirements include a stall speed (EAS) of ≤ 30 m/s (58 kts), an initial rate of climb ≥ 6.5 m/s (21 ft/s), a maximum ceiling of 6000 m (20000 ft), a

cruise speed of approximately 45 m/s (87 kts), endurance tailored to specific mission needs, and a line-of-sight range exceeding 150 km (81 nm). The stall speed primarily impacts take-off and landing performance, but with the EASA classification of UAVs using the "Equivalent Energy" criteria, it could directly influence airworthiness standards for civilian type certification [3]. Numerous articles and studies have explored the influence of aerodynamic forces on airfoils, focusing on the interaction between airfoil design and these forces. In one study conducted by Cistriani (2007), a comprehensive range of geometries was examined, optimizing two design points, and investigating stability at low Reynolds numbers, sensitivity to factors like free stream turbulence and in-flight icing. Wind tunnel tests were conducted on the two-dimensional wing section as well as the complete configuration of the UAV, validating the theoretical predictions. Finally, flight tests of the prototype aircraft were carried out, yielding results consistent with the previous design and testing efforts [4].

In a study conducted by Shah et al. (2013), the effects of air flow around solid objects were examined using a Wind Tunnel Testing Machine (WTTM) for aerodynamic research purposes. This machine consists of a closed tubular passage with the object being tested positioned at the center, accompanied by a powerful fan system that propels air past the object. The wing, or airfoil, generates lift by creating a pressure differential where the pressure above the wing is lower than that below it. Readings were collected on an airfoil model within the Wind Tunnel Testing Machine (WTTM) at various air speeds (20m/sec, 25m/sec, and 30m/sec) and different angles of attack (0°, 50°, 100°, 150°, 200°). To measure air velocity and pressure in the wind tunnel, measuring instruments like an anemometer and a multitube manometer were employed. Additionally, surface roughness testers were utilized to assess the roughness of the airfoil's surface, while Thermal Imaging Cameras were employed to capture the heat signature of the model being tested. Computational Fluid Dynamics (CFD) analysis was also conducted, examining different airfoil angles and velocity sections. The findings indicated that the airfoil model performed optimally when the angle of attack was set to 100° [5].

In another study by Kodavanla et al. (2017), the aerodynamic characteristics of the Lockheed Martin F-16 Fighting Falcon wing were evaluated using various numerical techniques across a range of angles of attack. The project involved creating a computational model of the F-16 wing within a finite computational domain, segmenting the domain into discrete intervals, applying boundary conditions such as Mach number and angles, and generating plots and results for parameters like the coefficient of pressure, lift coefficient, and drag coefficient. CFD simulations were performed under subsonic, transonic, and supersonic flight conditions. Finally, optimized results for lift and drag forces were obtained [6 and 7].

RESULTS AND DISCUSSION

This section presents a comparative analysis of the aerodynamic performance between the NACA 4412 and Falco UAV airfoils. The study utilizes relevant aerodynamic data, including airfoil shapes, coordinate points, viscous models, and boundary conditions, to ensure accurate results. The objective is to identify the optimal airfoil design for drones and unmanned aerial vehicles, particularly focusing on high-speed performance.

Simulation studies were conducted to compare these airfoils and determine the most suitable design for UAV applications. The evaluation considered various factors such as lift and drag

coefficients, as well as lift/drag ratios. A Mach number of 0.05245 and defined boundary constraints were utilized during the analysis, leading to the selection of the Falco airfoil as the preferred design. Ansys Fluent's computational fluid dynamics analysis played a crucial role in optimizing and assessing the performance of the airfoils.

To predict the aerodynamic characteristics at a Reynolds number of 1,191,185, a typical k-epsilon viscous model with enhanced wall treatment was employed. The comparison of data revealed that the airfoil design for surveillance drones demonstrated the highest efficiency.

The generation of grids and subsequent CFD analysis were performed on a 2D airfoil model constructed from the provided airfoil coordinates. A computational domain of the c-type was established around the model. The airfoils used in this research had a one-meter chord length, 100 percent line thickness, and 2.5 percent camber, serving as the parameters for the analysis [14-18].

As mentioned before, the main objective of the present work is to propose an airfoil design that achieves favorable lift coefficients and acceptable drag in fluid flows characterized by both low and high Reynolds numbers. To mitigate the occurrence of strong suction peaks at the leading edge, the nose shape parameter of the Falco UAV airfoil was significantly optimized. Furthermore, refining the overall contour of the airfoil involved addressing minor irregularities in curvature. The design also took into account the compatibility with composite materials commonly used in wing construction, which necessitated a thin trailing edge.

To assess the airfoil's performance and resilience under real-world operating conditions, comprehensive in-flight evaluations involving various leading-edge disturbances are highly recommended [16-18]. The research encompasses a complete process, starting with the establishment of appropriate specifications and concluding with flight testing. Intermediate stages involve CFD analysis and wind tunnel tests, providing valuable insights into flow behavior under different flow conditions. By considering the results obtained from various analytical and testing procedures, a robust connection can be established to comprehensively understand the behavior of the airfoil. Table 1 shows the results of C_d and C_l for NACA 4412, while figure 1 shows Cl and C_d Coefficients vs. AOA of NACA 4412 airfoil

Table 1.Results of C_d and C_l for NACA 4412

Angle of Attack	Lift coefficient (Cl)	Drag coefficient (Cd)
0	1.683	0.11
2	0.567	0.0137
6	0.943	0.0175
8	1.113	0.021
12	1.3376	0.04

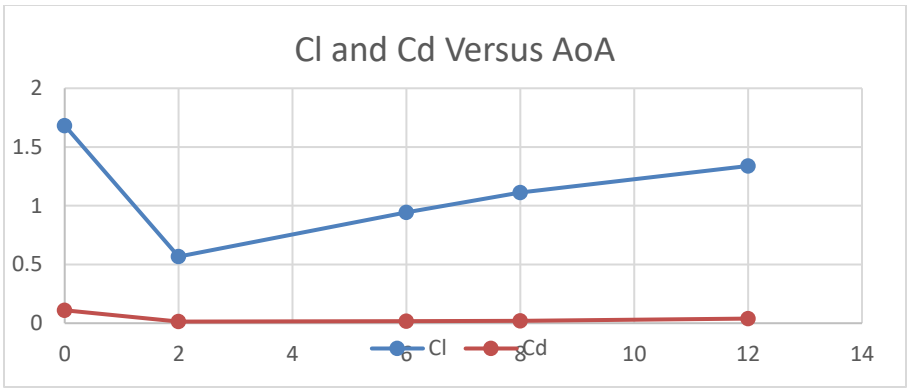

Figure 1. Cl and C_d vs. AOA of NACA 4412 airfoil

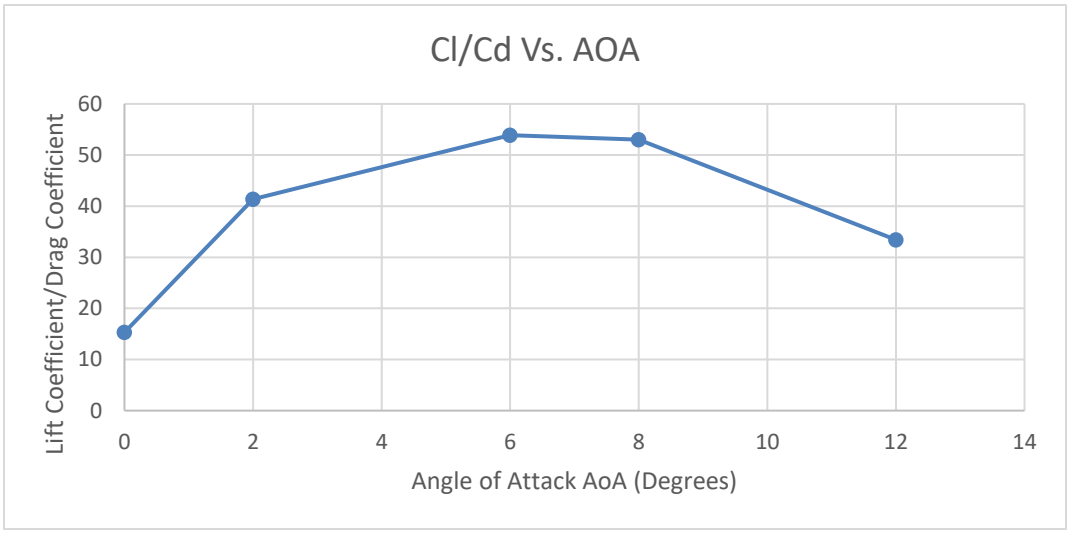

Figure 2. CD/CL vs. AOA

Figure 2 illustrates the impact of the angle of attack on the ratio of the lift coefficient to drag coefficient. It is evident that within the given range, the Cl/Cd ratio exhibits an upward trend as the angle of attack increases, peaking at 6 degrees. However, beyond this point, an inverse relationship emerges, leading to a decline in the Lift/Drag ratio as the angle of attack further increases.

Geometry Modeling

During the CFD analyses, a highly refined structured meshing technique was applied to all geometries. This meshing approach discretized the geometry into 140,901 nodes and 140,200 elements. The CFD evaluations of the NACA 4412 UAV airfoil and the Falco UAV airfoil presented here were compared with experimental findings documented in the literature. The use of the classic k-epsilon viscous model at high Reynolds numbers yielded remarkably accurate predictions of lift, drag, and overall aerodynamic performance. In the context of airflow, the desire is to have an airfoil that exhibits a high lift-to-drag ratio, as this characteristic enables UAVs to fly efficiently. When the pressure beneath the wing exceeds the force above the flap, a net upward force is generated, facilitating upward movement. For this study, airfoils with similar upper and lower surfaces, as well

as comparable mean camber line and chord line, were utilized. The primary objective of this research is to determine which airfoil exhibits the most optimal aerodynamic performance for drone applications. By utilizing CFD methods for fluid flow analysis around the airfoil, this research saves time and resources by reducing the reliance on practical tests. The precise simulation results were achieved through meticulous mesh refinement, particularly in the wall area. Figures 2 to 6 illustrate the geometry of the Falco airfoil and the corresponding CFD meshing.

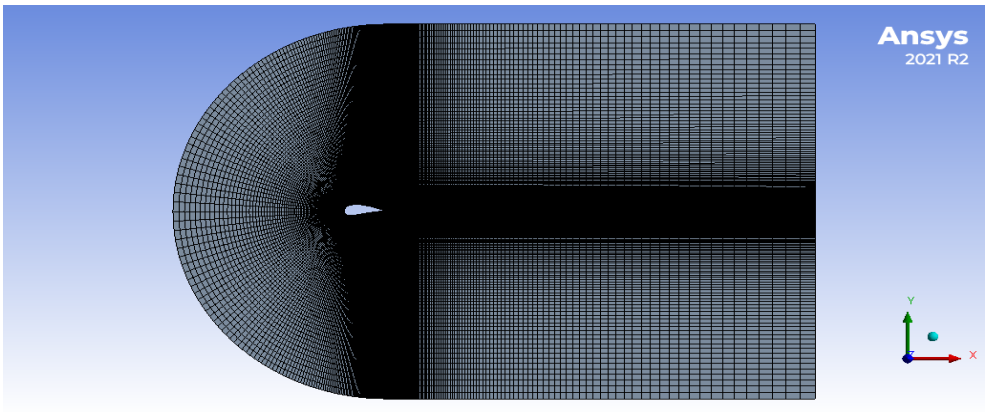

Figure 3. Structured meshing of Falco UAV airfoil geometry

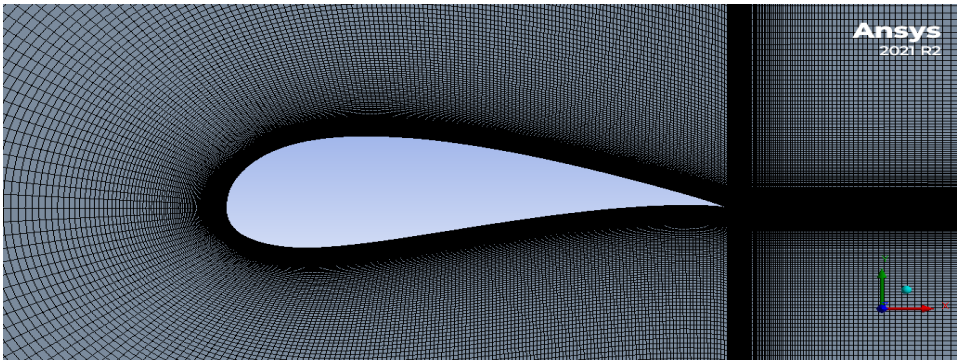

Figure 4. Meshing around Falco UAV airfoil

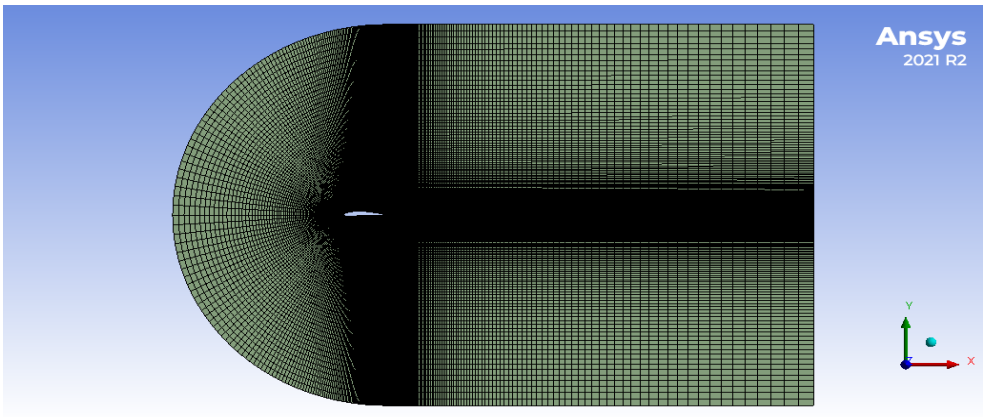

Figure 5. Structured meshing of NACA 4412 airfoil geometry

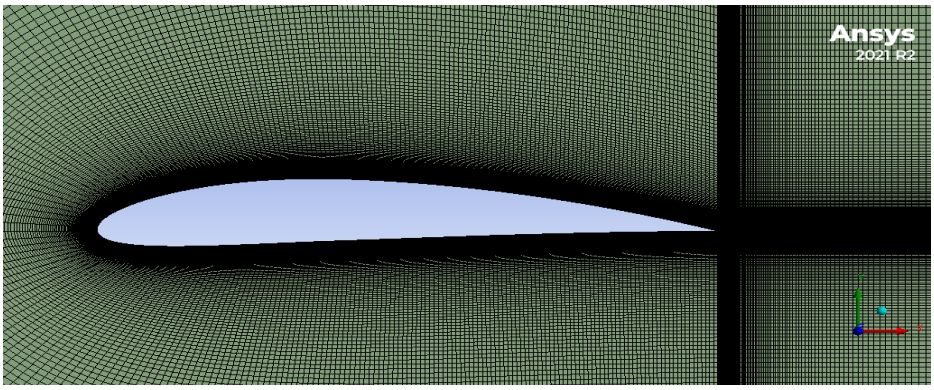

Figure 6. Meshing around NACA 4412 airfoil

CFD ANALYSIS

In this study, a steady-state, pressure-based solver, and finite volume discretization were employed to solve the governing equations of the k-epsilon model. The numerical solution error was carefully monitored by the designers to ensure proper convergence. A C-type computational domain with a radius of 5 m and a length of 10 m was selected for the simulations. Air characterized by a density of 1.225 kg/m^3 and dynamic viscosity of 1.7894 x10^{-5}Pa.s, was used as the fluid medium in the simulations. To establish mesh independence, grids of varying sizes were employed, increasing the number of grid elements until the solution exhibited minimal changes with further increases in mesh density. The convergence speed during the iteration phase was evaluated by examining the residuals of the governing differential equation's outcome variable. Additionally, the relative differences between two consecutive iterations were analyzed to verify convergence for each of the incorporated force coefficients. A 2D analysis was conducted in double precision, utilizing the normal k-epsilon flow equations to simulate the continuous flow of air around the aircraft's perimeter. The lift force is determined by the spacecraft's weight, while the drag force depends on the airplane's aerodynamic efficiency and wingspan.Table 2 presents the boundary conditions that were applied to these airfoils, providing essential information for the simulations.

Table 2. Boundary conditions applied.

Air density	1.225 kg/m3
Viscosity	1.7894e-05 kg/m-s
Inlet velocity	18 m/s
Wall Motion	Stationary Wall
Shear Condition	No Slip
Outlet Gauge Pressure	0 Pa
Pressure-Velocity Scheme	Coupled
Pressure, Momentum, Turbulent kinetic energy & dissipation rate	Second-order upwind
Gradient	Least Square Cell-Based

In this instance, a C-type finite element model was employed, where the radius and downstream length of the domain were both 10 times larger than the chord length. Efforts were made to control the proximity of the mesh elements surrounding the airfoil by adjusting the Y+ value to be smaller

than 1, ensuring a finer resolution near the surface. As for the boundary conditions, atmospheric pressure was used for both the inlet and outlet flows in this experiment.Figure 7 illustrates the pressure coefficient distribution around the airfoil shape, providing insights into the aerodynamic behavior.

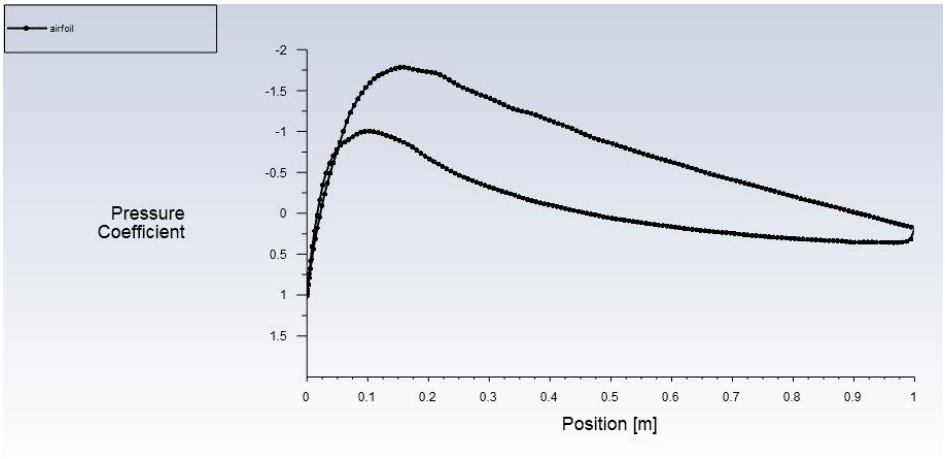

Figure 7. Pressure coefficient chart around the airfoil shape

To address this problem and simulate the influence on the surface of the airfoil, this study utilized fluid mechanics procedures, equations, and approaches. Crafting an efficient aerodynamic airfoil design holds utmost importance in the field of aviation to ensure its optimal performance during operational deployment. The CFD analysis outcomes for both Falco and NACA 4412 airfoils are presented in Table 3.

Table 3. CFD analyses results

Airfoil type	Falco		NACA 4412	
AOA	Cl	Cd	Cl	Cd
0	0.69413371	0.022814988	0.42027683	0.014777025
4	1.1256138	0.028992575	0.8183559	0.020894877
8	1.5060024	0.03926867	1.1828609	0.034394757
12	1.780155	0.055689057	1.4434187	0.058565944

In Figure 8, the pressure distribution surrounding the Falco airfoil at a 0-degree angle of attack (AoA) is illustrated. As expected, the highest pressure was observed at the front of the airfoil, specifically at the stagnation point where the fluid velocity decreases to zero. This pressure registered at 200 Pa. On the other hand, the upper surface of the airfoil recorded the lowest pressure of -350 Pa, specifically in a region that constitutes 0.2 of the total length. Furthermore, a pressure of -75 Pa was noted on the lower surface, resulting in a pressure difference of 275 Pa between the lower and upper surfacesof theairfoil.

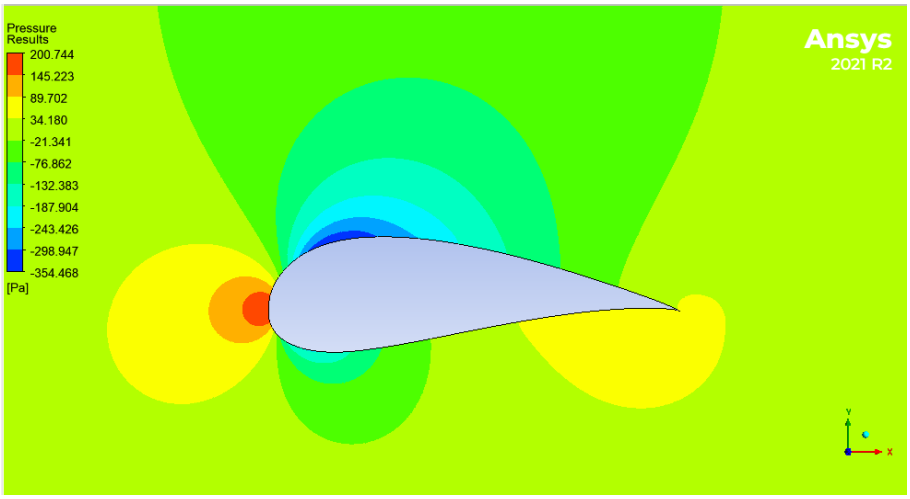

Figure 8. Pressure distribution around Falco airfoil at 0 deg AoA

In Figure 9, the pressure distribution around the NACA 4412 airfoil at a 0-degree angle of attack (AoA) is depicted. It is worth noting that the highest pressure of 188 Pa was measured at the leading edge of the airfoil. Conversely, the upper surface of the airfoil registered a pressure of -140 Pa, while the lower surface had a pressure of 22 Pa. Therefore, there is a pressure difference of approximately 160 Pa between the lower and upper surfaces.

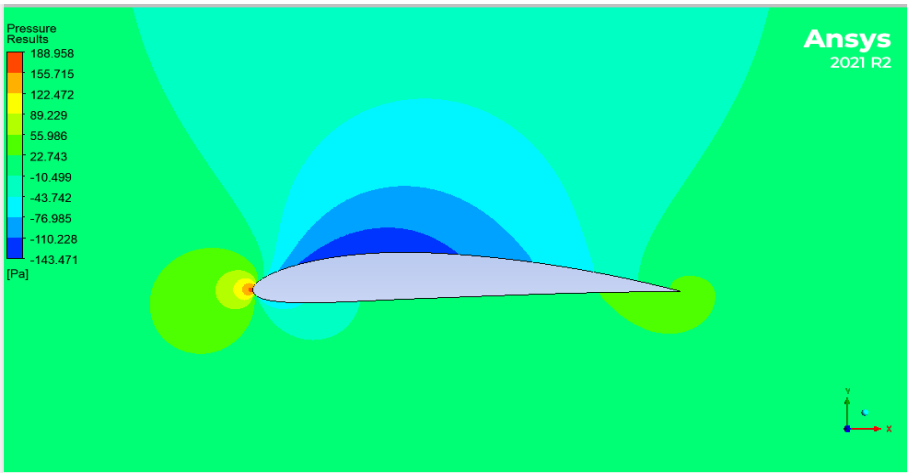

Figure 9. Pressure distribution around NACA 4412 airfoil at 0 deg AoA

In Figure 10, the velocity distribution around the Falco airfoil at a 0-degree angle of attack (AoA) is presented. Observing the figure, it becomes evident that the fluid velocity reaches zero at the leading edge of the airfoil, while a relatively lower velocity is observed at the trailing edge. Additionally, the maximum velocity of 29 m/s is found at the location where the minimum pressure is located, specifically on the upper surface of the airfoil. On the other hand, a velocity of 14 m/s was measured on the lower surface of the airfoil.

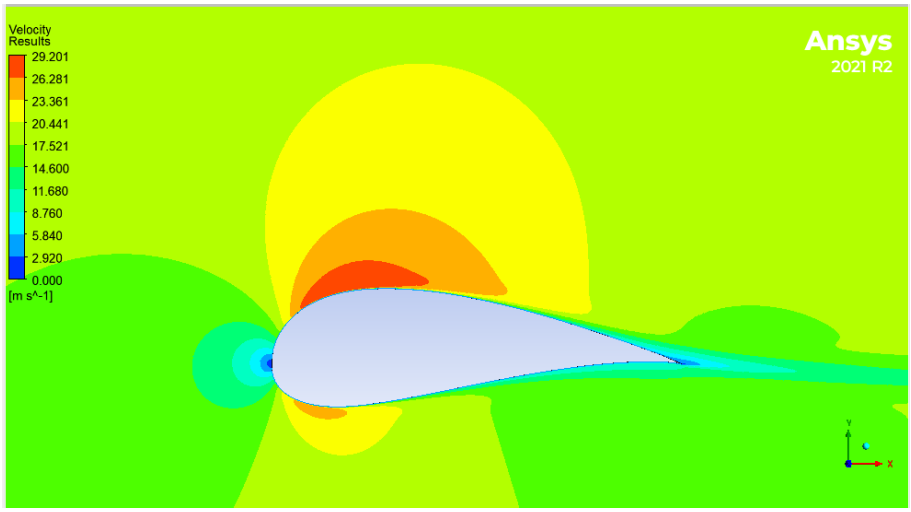

Figure 10. Velocity distribution around Falco airfoil at 0 deg AoA

Figure 11 illustrates the velocity distribution around the NACA 4412 airfoil at a 0-degree angle of attack (AoA). Upon observing the figure, it becomes apparent that the fluid velocity reaches zero at the leading edge of the airfoil, while a comparatively lower velocity is observed at the trailing edge. Moreover, the upper surface of the airfoil exhibits the maximum velocity, measuring 23 m/s at the location coinciding with the minimum pressure. In contrast, the lower surface of the airfoil records a velocity of 14 m/s.

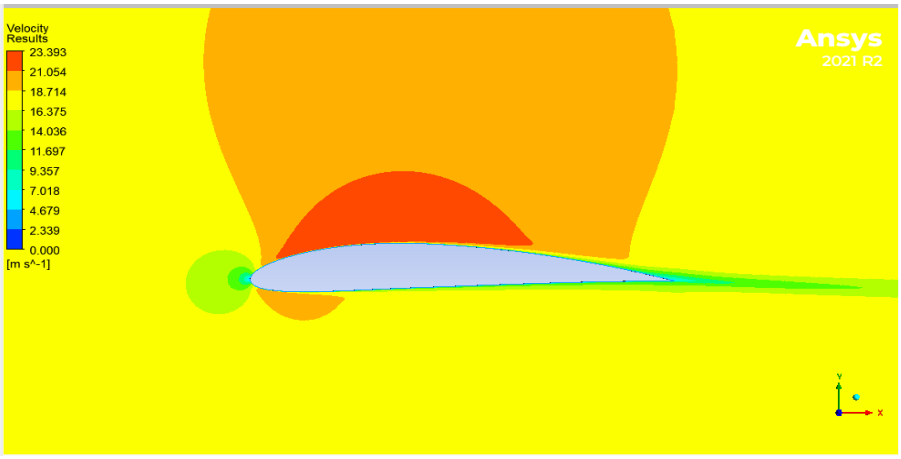

Figure 11. Velocity distribution around NACA 4412 airfoil at 0 deg AoA

The pressure contours clearly indicate that the top surface of the airfoil is subjected to low pressure, while the lower surface experiences high pressure. Additionally, there is an increase in velocity along the leading edge and a decrease in velocity along the trailing edge. The velocity distribution demonstrates that a lower angle of attack results in less lift compared to a higher angle of attack. The pressure distribution profiles reveal an augmentation of negative pressure on the top surface of the airfoil at higher angles of attack. Figures 12 to 15 exhibit the pressure and velocity distributions around the Falco and NACA 4412 airfoils at a 4-degree angle of attack (AoA).

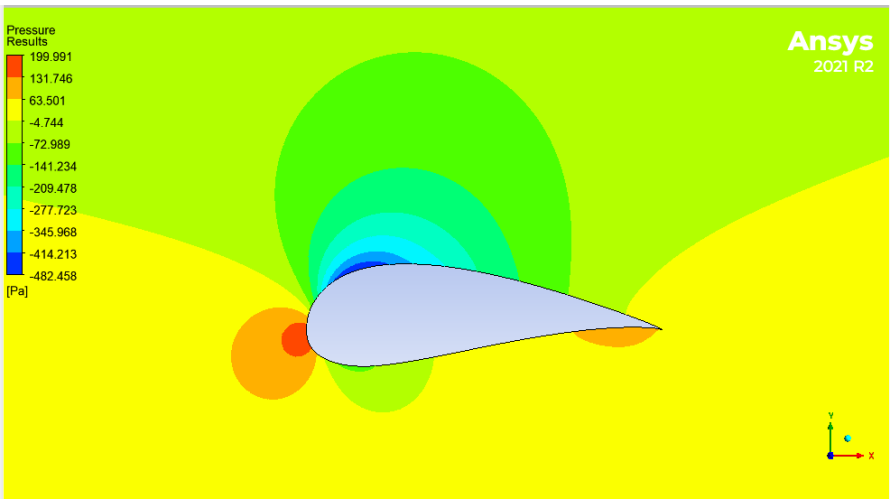

Figure 12. Pressure distribution around Falco airfoil at 4 deg AoA

Figure 12 provides an illustration of the pressure distribution around the Falco airfoil at a 4-degree angle of attack (AoA). As anticipated, the highest pressure was observed at the front of the airfoil, precisely at the stagnation point where the fluid velocity reaches zero. This pressure was measured at 200 Pa. Conversely, the upper surface of the airfoil exhibited the lowest pressure of -480 Pa, specifically in a region corresponding to 0.2 of the total length. Additionally, a pressure of -140 Pa was observed on the lower surface, resulting in a pressure difference of 340 Pa between the lower and upper surfaces of the airfoil. It is noteworthy that the pressure difference between the lower and upper surfaces of the airfoil increases from 275 to 340 Pa when comparing 0-degree and 4-degree AoA configurations.

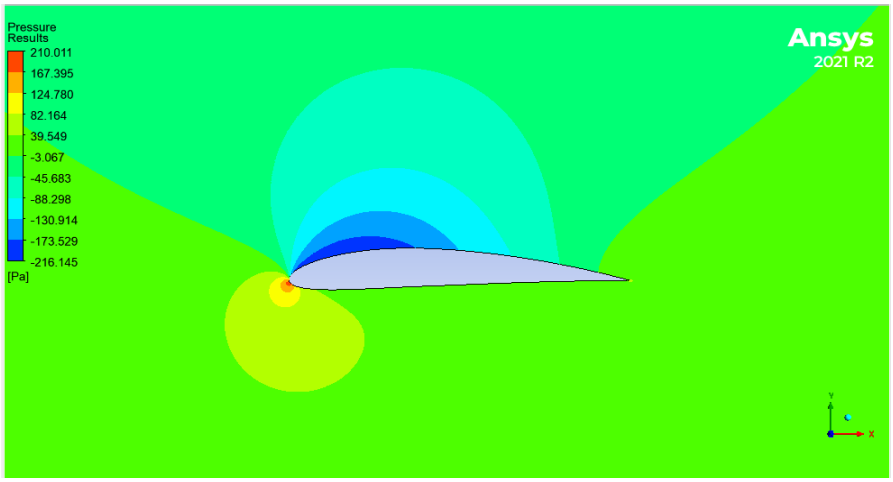

Figure 131. Pressure distribution around NACA 4412 airfoil at 4 deg AoA

Figure 13 illustrates the pressure distribution around the NACA 4412 airfoil at a 4-degree angle of attack (AoA). As expected, the highest pressure was observed at the front of the airfoil, precisely at the stagnation point where the fluid velocity reaches zero. This pressure was measured at 210 Pa. On the other hand, the upper surface of the airfoil displayed the lowest pressure, registering -216 Pa, particularly in a region that corresponds to 0.3 of the total length. Furthermore, the lower

surface experienced a pressure of -45 Pa, resulting in a pressure difference of 170 Pa between the lower and upper surfaces of the airfoil. Notably, when comparing the 0-degree and 4-degree AoA configurations, the pressure difference between the lower and upper surfaces of the airfoil increases from 160 to 170 Pa.

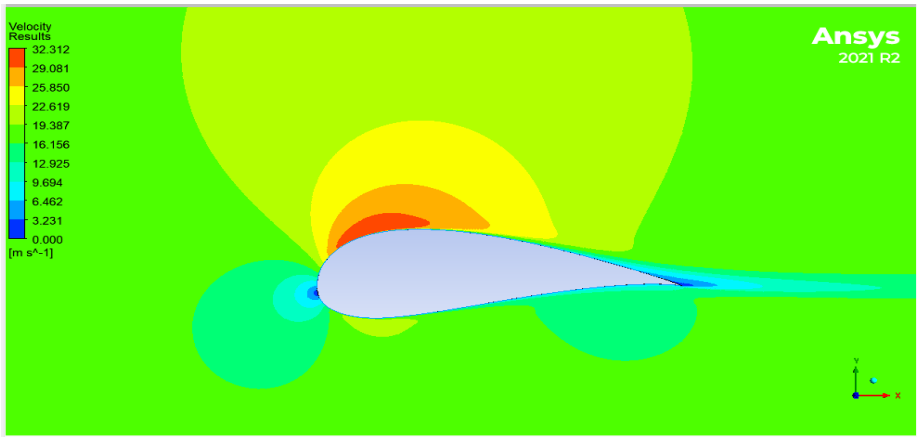

Figure14. Velocity distribution around Falco airfoil at 4 deg AoA

Figure 14 illustrates the velocity distribution around the Falco airfoil at 4 deg AoA. Upon observing the figure, it becomes apparent that the fluid velocity reaches zero at the leading edge of the airfoil, while a comparatively lower velocity is observed at the trailing edge. Moreover, the upper surface of the airfoil exhibits the maximum velocity, measuring 32 m/s at the location coinciding with the minimum pressure. In contrast, the lower surface of the airfoil records a velocity of (19-25) m/s.

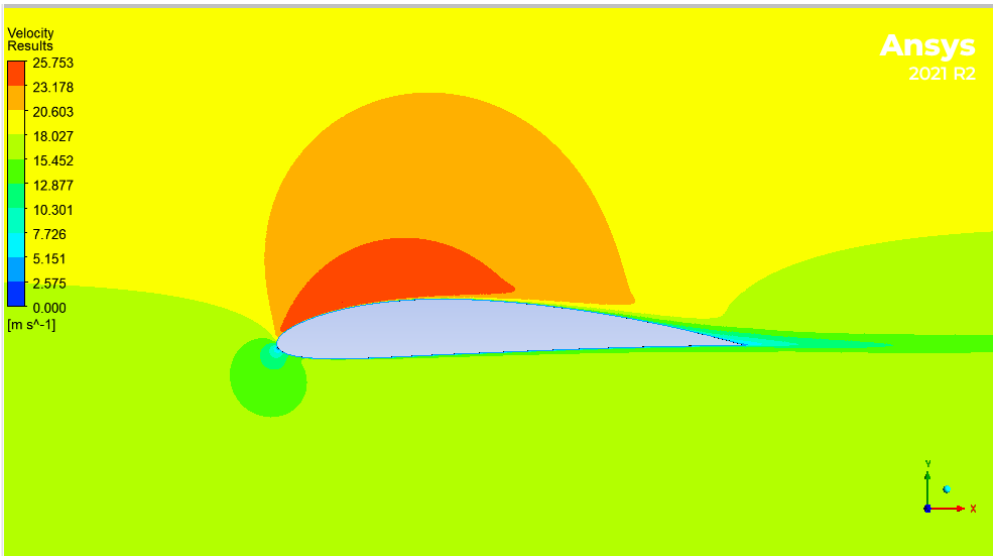

Figure15. Velocity distribution around NACA 4412 airfoil at 4 deg AoA

Figure 13 provides an illustration of the velocity distribution around the NACA 4412 airfoil at a 4-degree angle of attack (AoA). Upon examining the figure, it becomes evident that the fluid velocity becomes zero at the leading edge of the airfoil, while a relatively lower velocity is observed at the trailing edge. Furthermore, the upper surface of the airfoil displays the highest velocity, measuring

25 m/s at the location that aligns with the minimum pressure and spans across half of the airfoil's span. Conversely, the lower surface of the airfoil exhibits a velocity range of 12-15 m/s.Figures 16 to 19 show the Pressure and velocity distributions around Falco airfoil and NACA 4412 airfoils at 8 deg AoA.

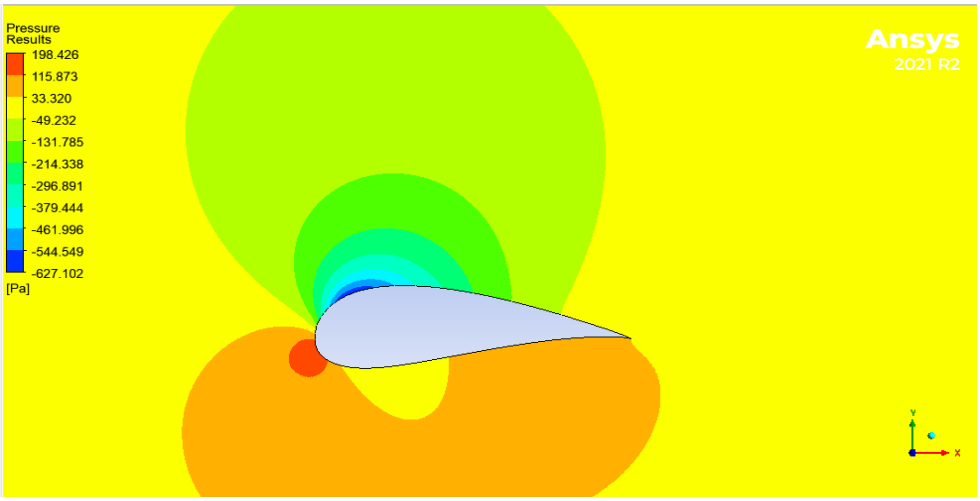

Figure16. Pressure distribution around Falco airfoil at 8 deg AoA

Figure 16 provides an illustration of the pressure distribution around the Falco airfoil at a 8-degree angle of attack (AoA). As anticipated, the highest pressure was observed at the front of the airfoil, precisely at the stagnation point where the fluid velocity reaches zero. This pressure was measured at 198 Pa. Conversely, the upper surface of the airfoil exhibited the lowest pressure of -620 Pa, specifically in a region corresponding to 0.2 of the total length. Additionally, a pressure of -40 Pa was observed on the lower surface, resulting in a pressure difference of 580 Pa between the lower and upper surfaces of the airfoil. It is noteworthy that the pressure difference between the lower and upper surfaces of the airfoil increases from 275 to 340 Pa to 580 Pa when comparing 0-degree, 4-degree, 8-degree AoA.

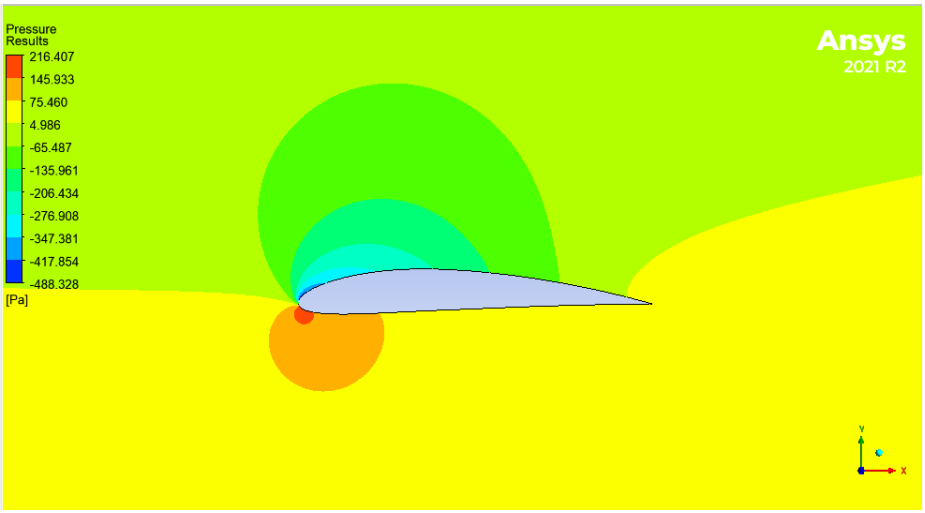

Figure17. Pressure distribution around NACA 4412 airfoil at 8 deg AoA

Figure 17 depicts the pressure distribution around the NACA 4412 airfoil at an 8-degree angle of attack (AoA). As expected, the highest pressure was observed at the front of the airfoil, precisely at the stagnation point where the fluid velocity reaches zero. This pressure was measured at 198 Pa. On the other hand, the upper surface of the airfoil exhibited the lowest pressure of -480 Pa, specifically in a region corresponding to 0.1 of the total length. Furthermore, a pressure of -75 Pa was observed on the lower surface, resulting in a pressure difference of 405 Pa between the lower and upper surfaces of the airfoil. Notably, the pressure difference between the lower and upper surfaces of the airfoil increases from 160 to 170 Pa for 0-degree and 4-degree AoA, and further increases to 405 Pa at an 8-degree AoA.

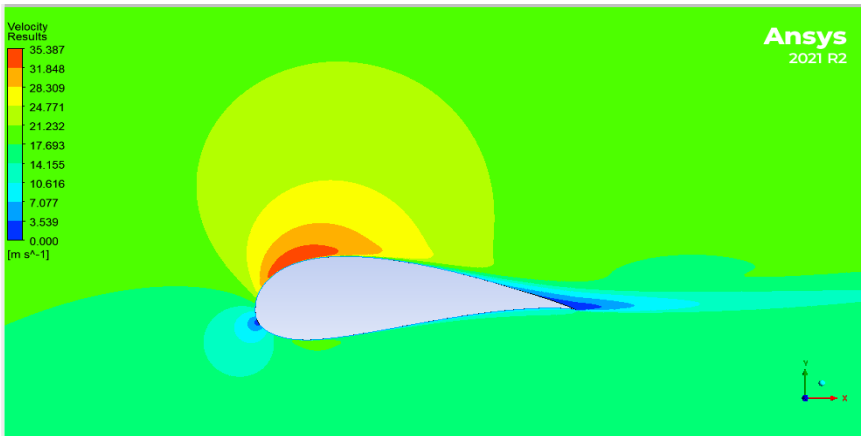

Figure 18. Velocity distribution around Falco airfoil at 8 deg AoA

Figure 18 presents an illustration of the velocity distribution around the Falco airfoil at a8-degree angle of attack (AoA). Upon examination of the figure, it becomes evident that the fluid velocity reaches zero at the leading edge of the airfoil, specifically at the stagnation point. Conversely, a relatively lower velocity of approximately 3.5 m/s is observed at the trailing edge. Furthermore, the upper surface of the airfoil exhibits maximum velocity, measuring 35 m/s at the location that aligns with the minimum pressure. In contrast, the lower surface of the airfoil records a velocity range of 14-21 m/s.

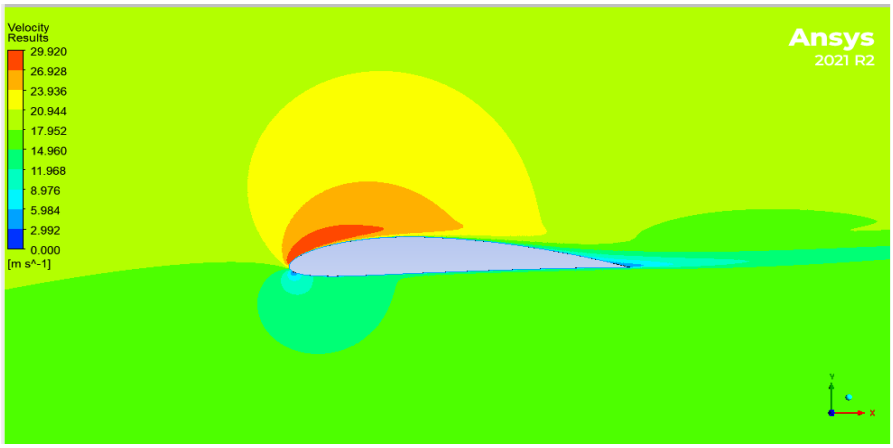

Figure 19. Velocity distribution around NACA 4412 airfoil at 8 deg AoA

Figure 19 provides an illustration of the velocity distribution around the NACA 4412 airfoil at a8-degree angle of attack (AoA). Upon examining the figure, it becomes evident that the fluid velocity becomes zero at the leading edge of the airfoil, while a relatively lower velocity is observed at the trailing edge. Furthermore, the upper surface of the airfoil displays the highest velocity, measuring 30 m/s at the location that aligns with the minimum pressure and spans across half of the airfoil's span. Conversely, the lower surface of the airfoil exhibits a velocity range of 9-17 m/s.

Figures 20 to 23 show the Pressure and velocity distributions around Falco airfoil and NACA 4412 airfoils at 12 deg AoA.

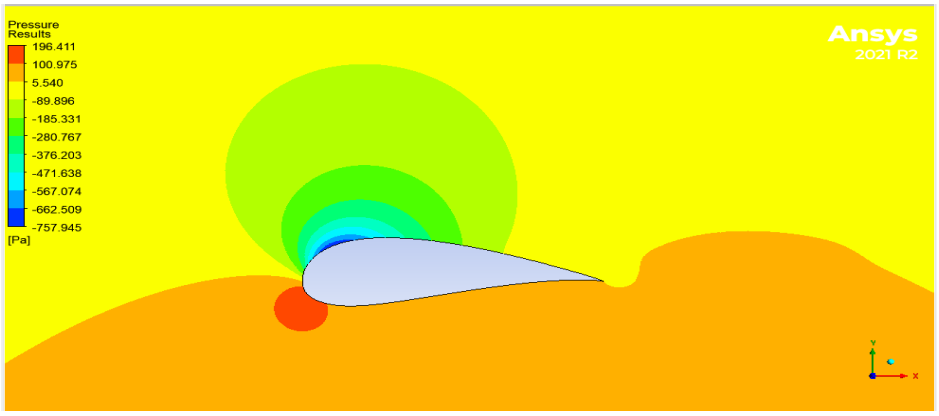

Figure20. Pressure distribution around Falco airfoil at 12 deg AoA

Figure 20 provides an illustration of the pressure distribution around the Falco airfoil at a 12-degree angle of attack (AoA). As anticipated, the highest pressure was observed at the front of the airfoil, precisely at the stagnation point where the fluid velocity reaches zero. This pressure was measured at 196 Pa. Conversely, the upper surface of the airfoil exhibited the lowest pressure of -750 Pa, specifically in a region corresponding to 0.2 of the total length. Additionally, a pressure of 100 Pa was observed on the lower surface, resulting in a pressure difference of 850 Pa between the lower and upper surfaces of the airfoil. It is noteworthy that the pressure difference between the lower and upper surfaces of the airfoil increases from 275 to 340 Pa to 580 Pa to 850 Pa when comparing 0-degree, 4-degree, 8-degree, and 12-degree AoA.

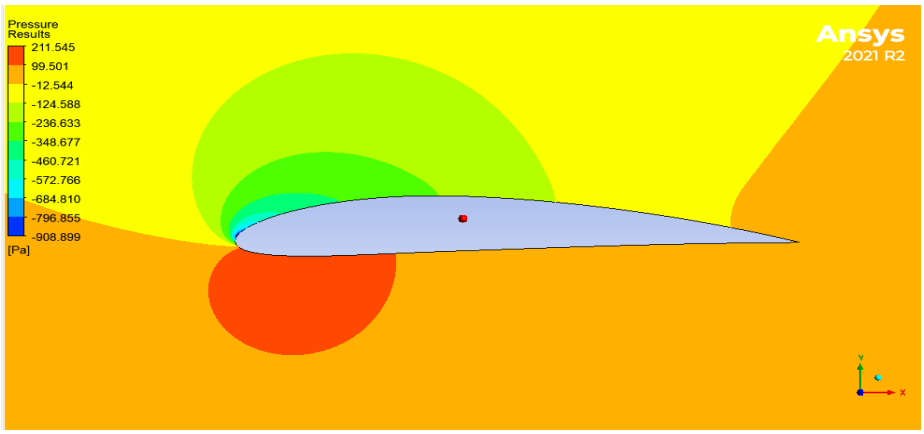

Figure 21. Pressure distribution around NACA 4412 airfoil at 12 deg AoA

Figure 21 depicts the pressure distribution around the NACA 4412 airfoil at an 12-degree angle of attack (AoA). As expected, the highest pressure was observed at the bottom of the airfoil, precisely at the stagnation point where the fluid velocity reaches zero. This pressure was measured at 210 Pa. On the other hand, the upper surface of the airfoil exhibited the lowest pressure of -350 Pa, specifically in a region corresponding to 0.1 of the total length. Furthermore, a pressure of 100 Pa was observed on the lower surface, resulting in a pressure difference of 450 Pa between the lower and upper surfaces of the airfoil. Notably, the pressure difference between the lower and upper surfaces of the airfoil increases from 160 to 170 Pa, and 405 Pa for 0-degree, 4-degree, and 8-degree AoA, respectively, and further increases to 450 Pa at an 12-degree AoA.

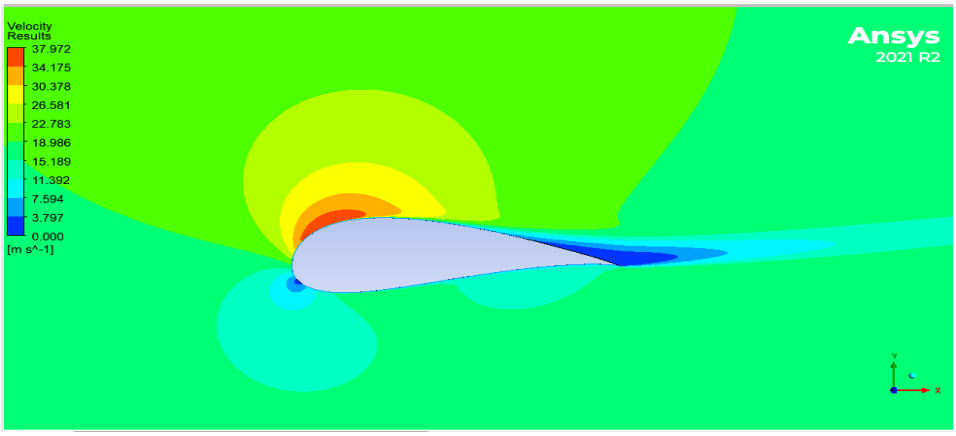

Figure 22. Velocity distribution around Falco airfoil at 12 deg AoA

Figure 22 presents an illustration of the velocity distribution around the Falco airfoil at a 12-degree angle of attack (AoA). Upon examination of the figure, it becomes evident that the fluid velocity reaches zero at the leading edge of the airfoil, specifically at the stagnation point and at the trailing edge of the foil. Furthermore, the upper surface of the airfoil exhibits maximum velocity, measuring 38 m/s at the location that aligns with the minimum pressure. In contrast, the lower surface of the airfoil records a velocity range of 11-19 m/s.

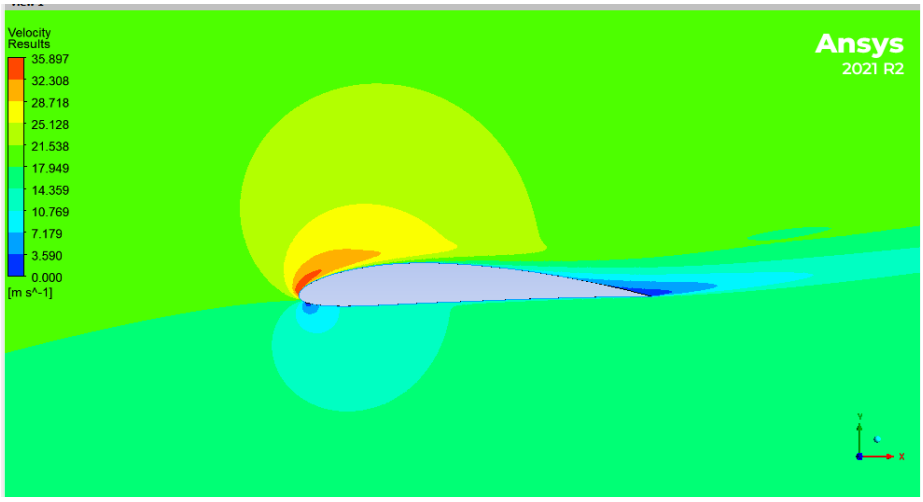

Figure 23. Velocity distribution around NACA 4412 airfoil at 12 deg AoA

Figure 23 provides an illustration of the velocity distribution around the NACA 4412 airfoil at a 12-degree angle of attack (AoA). Upon examining the figure, it becomes evident that the fluid velocity becomes zero at the bottom edge of the airfoil, while a relatively lower velocity is observed at the trailing edge. Furthermore, the upper surface of the airfoil displays the highest velocity, measuring 36 m/s at the location that aligns with the minimum pressure and spans across half of the airfoil's span. Conversely, the lower surface of the airfoil exhibits a velocity range of 14-18 m/s.

The lift coefficient of an airfoil can be significantly enhanced by utilizing the curvature formed by the leading-edge flap. One effective approach to improve the lift coefficient involves increasing the angle of attack until it reaches an optimal value, which can be determined through computational fluid dynamics analysis. Through this investigation, it was found that an angle of attack of 8 degrees achieves a satisfactory lift coefficient. Designers typically aim to maximize the lift-to-drag ratio by increasing the angle of attack, the airfoil thickness, the airfoil area, and the airspeed. Additionally, the camber of the airfoil plays a crucial role in determining the lift force.

Comparison of the Two Airfoils

Table 4 shows a Lift/Drag comparison between Falco and NACA 4412 airfoils.

Table 4. Lift/Drag ratio comparison.

AOA	Falco	NACA4412
0	30.42	28.44
4	38.82	39.17
8	38.35	34.39
12	31.97	24.65

Figure 24 shows a Lift-to-Drag ratio comparison between Falco and NACA 4412 airfoils.

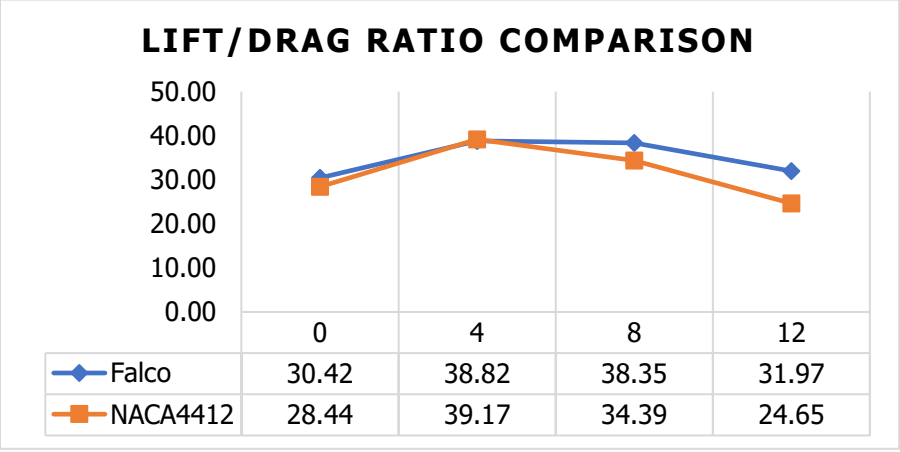

Figure 24. Lift-to-Drag ratio comparison chart.

The Falco airfoil exhibits a superior lift-to-drag ratio compared to the NACA 4412 airfoil, peaking at an angle of attack of 12 degrees before gradually decreasing. However, at 4 and 8 degrees of angle

of attack (AoAs), the lift-to-drag ratio is higher, but it diminishes as the boundary flow separates. When the AoA exceeds 10 degrees, the NACA 4412 aircraft experiences poorer aerodynamic performance, resulting in a lower lift-to-drag ratio. In a fluid medium, drag force opposes the motion of an object and reduces its lift, acting in the opposite direction. The velocity, air compressibility, viscosity, and size and shape of the object all contribute to the generation of drag in a flow.

CFD findings for the Falco airfoil show a considerable increase in lift coefficient values when compared to those for the NACA 4412 airfoil, which has a lower angle of attack. Although the lift coefficient rises as the attack angle increases, the drag coefficient also rises, and the total life to drag ratio decreases as the attack angle becomes higher. So, the angle of attack should not exceed 15 degrees. Using a Falco airfoil to construct the wings of an unmanned aerial vehicle (UAV) ensures that an acceptable amount of lift is created within the drone's stated boundary conditions. The lift-to-drag ratio is the most critical consideration for good wing aerodynamic design.Figure 25 shows Drag Coefficient of the two airfoils NACA 4412and Falco airfoils.

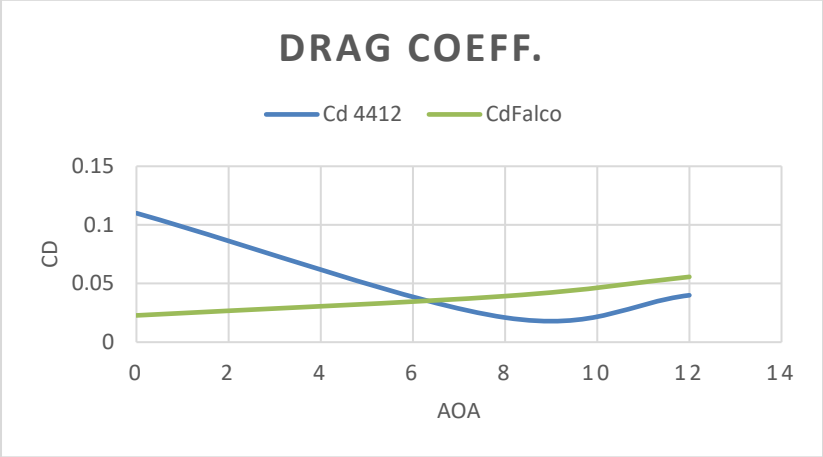

Figure 25. Drag Coefficient of the two airfoils NACA 4412 and Falco airfoils

Figure 26shows lift coefficient of the two airfoils NACA 4412 and Falco airfoils.

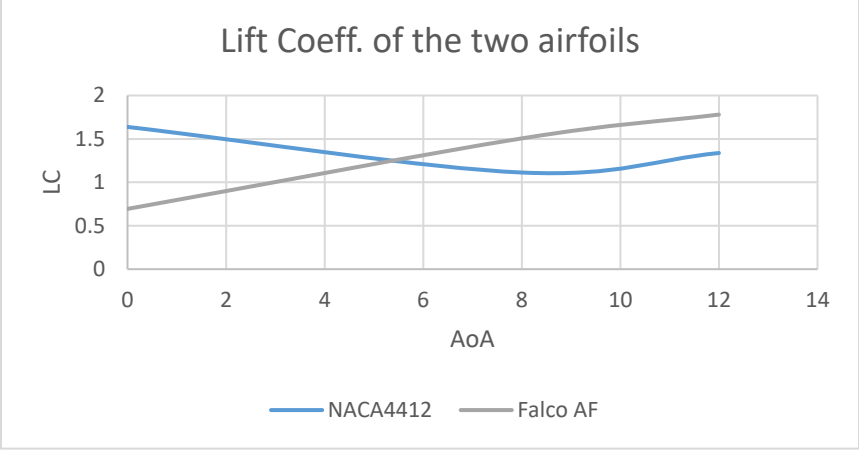

Figure 26.Lift coefficient of the two airfoils NACA 4412 and Falco airfoils.

It can be noticed that drag coefficient for Falco airfoil is lower than NACA 4412 till 6 degrees (AoA) but after 6 degrees it becomes higher than NACA4412. For the lift coefficient below 5 degrees of AoA, the lift coefficient of Falco is higher than that NACA 4412, after 5 degrees AoA it becomes higher than NACA 4412 foils.

Conclusions

A comparative study of various airfoils recommended the use of the Falco airfoil for drone applications due to its high lift-to-drag ratio. The study employed computational simulation software ANSYS Fluent, which solved Navier-Stokes and energy equations to predict flow patterns around different airfoils (pressure distribution and velocity field). Among the tested airfoils, the Falco UAV airfoil exhibited superior lift coefficient and lift-to-drag ratio. Additionally, its drag coefficient remained within acceptable limits. The angle of attack played a crucial role in aerodynamic performance, with the highest values achieved at a 12° angle of attack. As the angle of attack increased, the location of low pressure and weak areas progressively shifted from the lower surface to the upper surface due to changes in flow separation. The study demonstrated that computational modeling using FLUENT could yield results as accurate as those obtained from wind tunnel experiments. Moreover, utilizing ANSYS Fluent not only provided precise results but also reduced costs by eliminating the need for a series of physical experiments.

References

[1] KSU (2017).Basic Aerodynamics. Category B1/B2 according to Part-66 Appendix 1-KSU.Issue 1. Pp: 1-74.

[2] Chandrala M., Abhishek Choubey (2012) “Bharat Gupta Aerodynamic Analysis of Horizontal Axis Wind Turbine Blade”, IJERA, Vol. 2, Issue6.

[3] Impact Energy Method for Establishing the Design Standards for UAV Systems, Appendix to JAA/ Euro-control UAV Task-Force Final Report, Enclosure 3, May 2004

[4] Cstriani, L. (2007) Falco UAV Low Reynolds Airfoil Design and Testing at Galileo Avionica. In UAV Design Processes / Design Criteria for Structures (pp. 3.3-1 – 3.3-24). Meeting Proceedings RTO-MP-AVT-145, Paper 3.3. Neuilly-sur-Seine, France: RTO.

[5]Shah I.M., S. A. Thakkar, K. H. Thakkar, Bhavesh A. Patel (2013). Performance Analysis on Airfoil Model in Wind Tunnel Testing Machine (WTTM).Engineering Research and Applications (IJERA), Vol. 3, Issue 4, Jul-Aug 2013, pp.2094-2103

[6]KodavanlaB., P K Dash, P Srinivas Rao (2017). Computational Aerodynamic Analysis of F-16 Falcon Wing.International Journal of Engineering Technology Science and Research IJETSR,Volume 4, Issue 11

[7]KodavanB., Sai Kiran Burra, G. Santosh, P. Srinivas Rao, P. Anudeep & V. Madhavi (2018). CFD ANALYSIS OF F-16 FALCON. International Journal of Mechanical and Production Engineering Research and Development (IJMPERD), Vol. 8, Issue 2, Apr 2018, 1293-1302.

[8] Diasinos S., Tracie J Barber, and Graham Doig (2012). Influence of wingspan on the aerodynamics of wings in ground effect. Proc IMechE Part G: J Aerospace Engineering 0(0) 1–5.

[9] Robin K. (2019). Design and Analysis of Dimple Arrangement on a Small Wind Turbine Blade. International Journal of Innovative Technology and Exploring Engineering (IJITEE) Volume-9 Issue-2.

[10] Reddy K., Bachu Deb, and Bidesh Roy (2021). Analysis of the Aerodynamic Characteristics of NREL S823 and DU 06-W-200 Airfoils at Various Reynolds Numbers Using Qblade. Emerging Trends in Mechanical Engineering, Lecture Notes in Mechanical Engineering, https://doi.org/10.1007/978-981-15-8304-9_20

[11] Kandwal S., and S. Singh, "Computational Fluid Dynamics Study of Fluid Flow and Aerodynamic Forces on an Airfoil," IJERT, Vol. 1 Issue 7, September – 2012.

[12] Logsdon N., "a procedure for numerically analyzing airfoils and Wing sections," The Faculty of the Department of Mechanical & Aerospace Engineering University of Missouri – Columbia, 2006.

[13] Tangler, J. L., & Somers, D. M. (1995). NREL airfoil families for HAWTs (No. NREL/TP-442-7109). National Renewable Energy Lab., Golden, CO (United States).

[14] S. V. Penumarthi, “CFD analysis on NACA 63-215 airfoil using ANSYS fluent for wind turbine,” Int. J. Res. Appl. Sci. Eng. Technol., vol. 8, no. 8, pp. 1336–1342, 2020.

[15] A. González and J. Hinojosa, “Study of the influence of protuberances in the trailing edge of airfoils and determination of their aerodynamic efficiency through CFD using Ansys Fluent,” Rev. Int. Metod. Numer. Calc. Disen. Ing., 2019.

[16] S. Wang et al., “Simulation analysis of airfoil deformation of agricultural UAV under airflow disturbance based on ANSYS,” IFAC-PapersOnline, vol. 51, no. 17, pp. 826–830, 2018.

[17] Z. L. Peng, “Flow field simulation of airfoil and analysis of vibration modal based on ANSYS,” Adv. Mat. Res., vol. 268–270, pp. 581–583, 2011.

[18] K. M. Almohammadi, “Assessment of several modeling strategies on the prediction of lift-drag coefficients of a NACA0012 airfoil at a moderate Reynold number,” Alex. Eng. J., vol. 61, no. 3, pp. 2242–2249.